Calibration of TimePix4 Detector for VELO in LHCb

Anna Gawehn

Supervisors: Edgar Lemos Cid, Mohammadtaghi Hajheidari

September, 2023

Abstract

The Timepix4 sensor module is a high-timing precision detector that is going to be build into the next update of the Vertex Locator (VELO) in LHCb. Currently, it exhibits a difference in gain of up to 2.5× across the sensor which is adverse when measuring the energy of charged particle. Up until now, the calibration process has only been proved for the Timepix3 [3]. Following a similar procedure as for the Timepix3 calibration, shortscan measurements to better identify the non-linear region of the detector and Fe55 and Cd109 measurements were conducted in order to verify the correction. The calibration process for the Timepix4 module (N10 in particular) was conducted successfully.

1. Introduction

VELOs current version was installed in LHCb in 2022 for the third run of LHC. It was developed to recreate the particles trajectories with a frequency of 40MHz only 5.1mm away collision point. The goal for next VELO (upgrade II) is to add timing to be able to disentangle the primary vertices, since the will be much more collisions. [7]

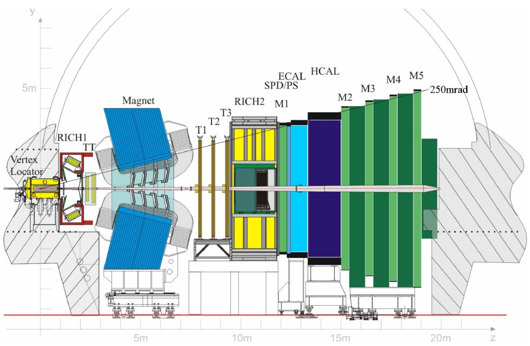

Figure 1: LHCb schematic, Vertex Locator (VELO) at the very left [1]

Timepix4 is the new generation of high-end detectors with high timing resolution, sensitivity and imaging quality. It is a hybrid silicon pixel detector that consists of 448×512 pixels each with a square pitch of $55\mu m$. This results in a 24.7×30.0 mm^2 area which can be tiled on all four sides. The planar sensors, which can be between 100 and $300\mu m$ thick, is solder bump bounded to the readout ASIC as can be seen in figure 2. The output of the data is realized with 2 to 16 serializers that run at an adjustable bandwidth between 40Mbps and 10 Gbps.

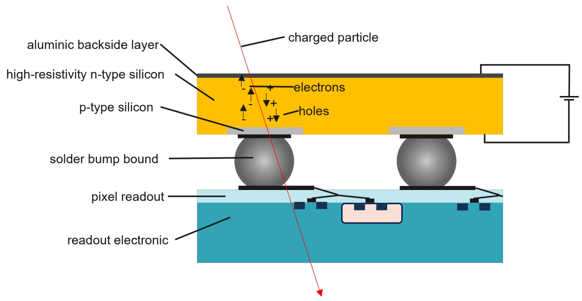

Figure 2: Schematic of Sensor

The detector can be operated in two different modes, data driven or frame based. In the data driven mode, which was used in the scope of this work to characterize the individual pixels, each pixel only reacts to a hit when the energy is above a certain predefined threshold that can be adjusted globally and locally. Upon a hit with an energy over threshold level, the time of arrival (ToA) and Time over Threshold (ToT) are obtained. For the ToT value, the duration of the signal pulse is measured as the longer the pulse duration, the more energy was absorbed (seen figure 3). In the data driven mode, the threshold for an individual pixel is at 0.8 to $1ke$ [2], the ionization energy of silicon is at 3.6 $\frac{eV}{e-h}$.

Motivation. Due to several reasons (power distribution across sensor, manufacturing variation, threshold calibration) the individual gain values across the chip differ up to 2.5× (see figure 4). This is undesirable behaviour when wanting to measure energy with the Timepix4.

In order to overcome the issue of gain differences, the following procedure was executed. First of all,

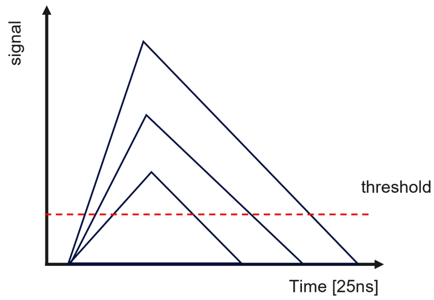

Figure 3: Time-over-Threshold (TOT)

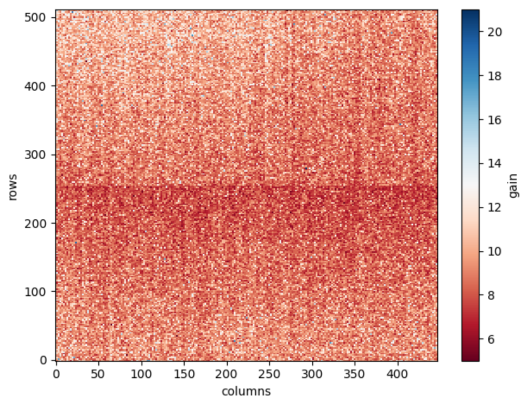

Figure 4: Gain distribution over entire detector

	Energy [keV]	Relative probability	Energy [ke]
Fe55 [6]	5.88 5.89	51 100	1.63
	6.49 6.53	20.5	1.81
Cd109 [5]	21.99 22.16	53.05 100	6.11
	24.94	27.7	6.93

Table 1: Energy of Fe55 and Cd109 radioactive source in [keV] and [ke] (combined peaks as to be seen in the gaussian fit)

injection measurements were conducted to characterize each individual pixel. The obtained data was then fitted with equation 1. Afterwards, radioactive source measurements with two different sources were done in order to be able to verify the correction. The inverse function was applied (eq. 2) to correct the pixels and convert the obtained source energy from ToT to keV. The results then were corrected with a shift factor.
Overall it was proven, that the calibration process as conducted in this report works well for Timepix4.

2. Data collection

Test pulse injection measurements. Each pixel of the
Timepix4 module has an intrinsic injection circuit which can be used to iteratively inject charge into a pixel and measure the obtained signal response in form of ToT value per event. For the measurements, the sensor was mounted on a Spidr4 readout board. The setup was measured in a climate chamber at 20°C and the sensor itself was depleted with 60V.

For the longscan measurements, the region between 1 and 4ke was measured with steps of Δ0.2ke to better identify the non-linearity (up to 2ke). The linear region from 4.5 to 16ke was measured with Δ0.5ke. This pattern results in overall 40 injection steps per run, where each injection step is executed 50 times to ensure sufficient data for statistics. This process is done simultaneously for 896 pixels with a distance of 16 pixels per row/column. As a result, there are 256 runs needed to characterize each pixel on the sensor, this process takes about 15 hours for the entire ASIC. The same process was done for the non-linear region close to the threshold with fine grained measurement steps of Δ0.05ke between 1 and 4ke.

Source measurements. The source measurements are conducted in order to verify that the entire fitting and data correction process works correctly. Two sources were used, Fe55 [6] and Cd109 [5]. The energy of Fe55 is only slightly above the pixel threshold of 1ke with 1.63 and 1.81ke for both peaks (see table 1). As already mentioned before, the non-linear behaviour of a pixel is up to about 2ke, hence Fe55 is in this non-linear region. Therefore, Cd109 was selected for a second measurement, since the two peaks are at 6.11 and 6.93ke (linear region). The two peaks are also further apart, which makes it possible to Gaussian fit both peaks individually and determine their energy with the calibrated sensor.
The setup itself was not changed, the sensor, ASIC and readout electronic remained in the climate chamber at 20°C and the same depletion charge was applied as for the injection measurements. In order to be able to use the source verification for the same pixels, the sources were adjusted by hand to cover the same region on the detector.
For Fe55 about $1.07 * 10^7$ events were recorded and $2.4 * 10^7$ for Cd109. In both cases only events with a cluster size of one were selected for analysis in order to rule out the cases where the energy of one particle was detected with two or more pixels (clustering).

3. Analysis

Test pulse injection measurements. To be able to use the characterization data from the long- and shortscan measurements, the data needs to be fitted. For the fitting, the following equation was used

$$ToT = a * Q_{inj} + b - \frac{c}{Q_{inj} - t} \quad (1)$$

as it was also used for the calibration of Timepix3 [3]. Having measured Q_{inj} and the according ToT values, the four fit parameters were obtained using pythons `curve_fit` function [4]

```
start = [9,0,3,.6]
bound = ([0,-10,0,0],[40,10,15,1.9])
curve_fit(func,steps,Q,p0=start,bounds=
  bound,sigma=E,absolute_sigma=True)
```

where `steps` is the above specified array of long- or shortscan charge injection steps. The error `E` was calculated with $\sigma/\sqrt{N_{inj}}$, where N_{inj} is equal to the amount of injections per step and σ denotes the standard derivation of each injection step, since each step is executed 50 times.

The visual results of the longscan data fit can be observed in figure 5, where the acquired data and the according fit function that was obtained as described above are displayed for two pixels.

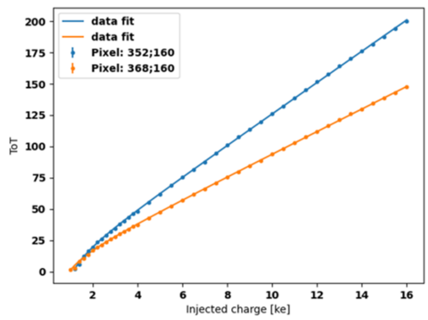

Figure 5: longscan injection measurement results for two different pixels and the fit

Figure 4 displays how gain parameters of each individual pixel are distributed along the entire sensor.

Source measurements. After having obtained the fit parameters with equation 1, the same parameters are used to identify the amout of deposited charge from the radioactive source in the according pixel. The algorithm finds all events for the given pixel (about 400-600 events at the closest distance from source to sensor). These events are registered as ToT values. With both the fit parameters and the ToT values, one can obtain the energy distribution for one pixel [3].

$$f^{-1}(ToT)[ke] = \frac{at+ToT-b+\sqrt{(b+at-ToT)^2+4ac}}{2a} \quad (2)$$

To obtain the results in keV, the obtained energy in ke has to be multiplied by the ionization energy of silicon is at 3.6 $\frac{eV}{e-h}$. Figure 6(a) displays two uncorrected pixels for Cd109 detection, one can very clearly see the impact of the gain difference of two different pixels. The pixel that is displayed with blue colour has a gain about 1.4× higher than the other pixel.
Figure 6(b) displays the energy distribution of the same pixels, but after the inverse function (eq. 2) and the ionization energy factor were applied.

4. Results

Long measurements. As a result it can be said, that the longscan measurements and the fitting quality with equation 1 was really good. Including the error in the fitting process, the χ^2 value was between 0.7 and 1.5, which is in a very good range.

Short measurements. The shortscan measurements on the other hand did not yield such good results. Using the same fit function as before, the χ^2 ranged anywhere from -200 to -10, depending on the pixel. After discarding the non-linear region and only using the data from 1.8-4.0ke, the χ^2 value was much improved (0.1-0.5) but trying to apply the obtained fit parameters on the longscan data, the fit was completely off (χ^2 of anywhere between -80 and 30). Thus, the shortscan measurements did not yield any further information about the non-linear behaviour of the pixel and the longscan fit parameters were used for all evaluation presented in the work.

Source measurements. Both source measurements were able to verify the calibration process, since they obtained the correct results after applying a general correction factor. In figure 7(a) and 7(c) the sum of 100 corrected pixels with Fe55 and Cd109 events (corrected with eq. 2) are displayed. As noted in the plots, μ_{Fe55} is at 6.35keV and μ_{Cd109} at 22.94 and 26.16keV. For Fe55 there are two expected peaks at 5.88 and 6.51keV, the latter one is much less significant. However, due to the closeness of the peaks only one is expected to be seen visually at 5.95keV. The measured and the expected mean of Fe55 differ in 6.72%.
A similar behaviour applies to Cd109, the measured peaks deviate from the expected peaks (22.09 and 25.19keV), which is a 3.76% and 3.7% shift, respectively.
Since both Fe55 and Cd109 have a systematic shift in the same direction while still having a good σ,

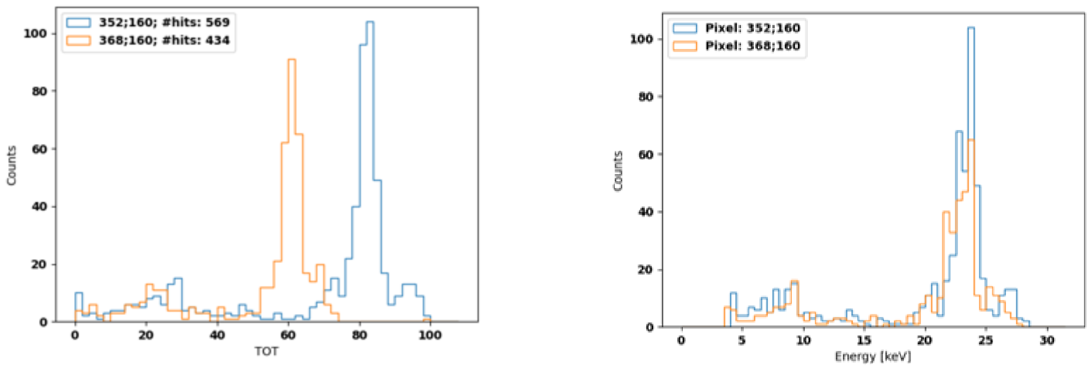

(a) uncorrected Cd109 events, ToT

(b) corrected Cd109 events, keV

Figure 6: 6(a) and 6(b) show two pixel with uncorrected and corrected gains, respectively

it was assumed that the shift is due to yet uncalibrated pixel capacitance. Therefore the gain parameters of each individual pixel could be corrected by the given factor. As a result, the obtained mean values were much better while still having a really good sigma, see figures 7(b) and 7(d) (σ of 1.36 and 0.96, respectively).

5. Conclusion

The shortscan measurements did not yield any imporved results about the non-linear region.
The different shift values of Fe55 with 6.72% and Cd109 with about 3.7% are probably due to the fact, that the energy of Fe55 is in the non-linear region with 1.63 and 1.81ke. Therefore, it is well justified having conducted the additional measurements with Cd109. They were able to verify the correctness of the calibration process. By adjusting the systematic shift it was possible to obtain the expected energy values with a good sigma. It can be said that the calibration process as explained in this report works correctly for the Timepix4.

6. Outlook

Due to the very limited time available for this project, there remain many possibilities to further investigate the specific behaviour and characterization of the Timepix4 sensor. The general shift of the corrected spectra may be due to the fact that the individual pixel capacitance was not yet determined. Doing so could result in a more exact energy detection. Moreover, the individual pixel threshold is not yet calibrated. This can be done by using the data that was already collected and observing the region very close to 1ke (the shortscan data could be used for this). Another option to identify the threshold is to iteratively increase the threshold for between 0.7 and 1.3ke for example to keep a record of when the pixel is enabled.
In addition to that, the minimum ionizing particle data from the test beam could be used to further verify the correctness of the fit.
As can be seen in figure 4, the gain differences are not completely arbitrary across the chip. Understanding why that is could also be subject of further research.

Acknowledgements

Thanks a lot to Mohammad Hajheidari and Edgar Lemos Cid for being such helpful and supporting supervisors.

I would also like to thank the committee of the Moritz Karbach Prize for selecting me as one of this year's winners.

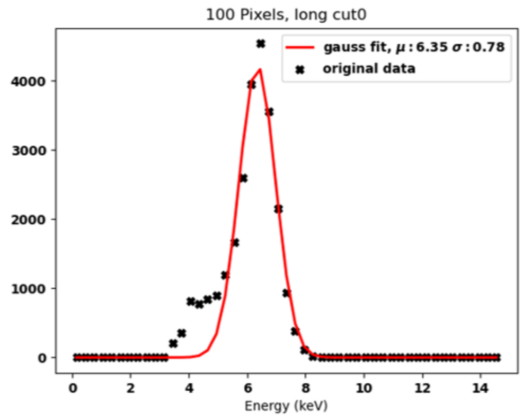

(a) Fe55, shift uncorrected

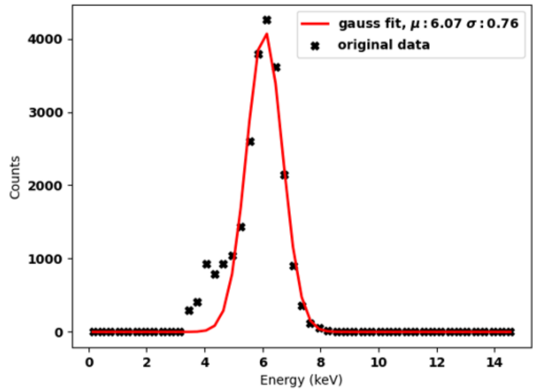

(b) Fe55, shift corrected with 6.72%

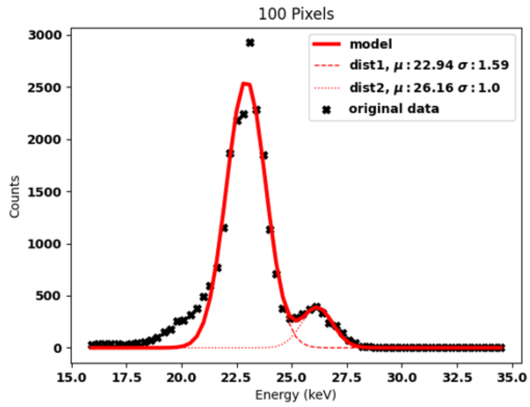

(c) Cd109, shift uncorrected

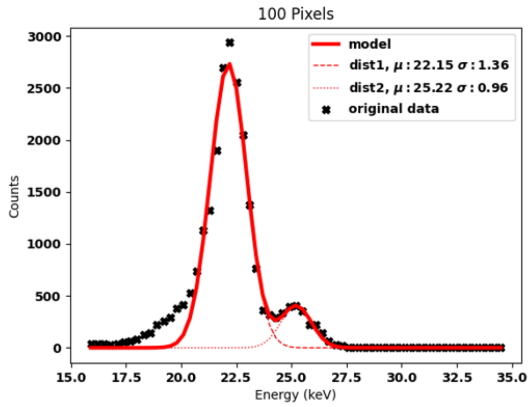

(d) Cd109, shift corrected with 3.76%

Figure 7: Plots over 100 pixels, data is corrected with fit parameters, 7(b) and 7(d) are systematically corrected, Cd109 cut off for better Gaussian fit

References

[1] LHCbcollaboration, ≪LHCb Detector Performance≫, Int. J. Mod. Phys. A **30**, 1530022 (2015) 10.1142/S0217751X15300227.

[2] X. Llopart, J. Alozy, R. Ballabriga, M. Campbell, R. Casanova, V. Gromov, E. Heijne, T. Poikela, E. Santin, V. Sriskaran, L. Tlustos, and A. Vitkovskiy, ≪Timepix4, a large area pixel detector readout chip which can be tiled on 4 sides providing sub-200 ps timestamp binning≫, Journal of Instrumentation **17**, C01044 (2022) 10.1088/1748-0221/17/01/C01044.

[3] F. M. Pitters, N. Alipour Tehrani, D. Dannheim, A. Fiergolski, D. Hynds, W. Klempt, X. Llopart Cudie, M. Munker, A. M. Nurnberg, S. Spannagel, and M. J. Williams, ≪Time and energy calibration of timepix3 assemblies with thin silicon sensors≫, (2018).

[4] *Python curve_fit*, https://docs.scipy.org/doc/scipy/reference/generated/scipy.optimize.curve$_fit.html$, Accessed: 2023-09-11.

[5] *Table de radionucléides* $^{109}_{48}Cd_{61}$, BNM - LNHB/CEA (1996-2004).

[6] *Table de radionucléides* $^{55}_{26}Fe_{29}$, BNM - LNHB/CEA (1996-2004).

[7] *The new lhcb velo*, https://home.cern/news/news/experiments/new-lhcb-velo, Accessed: 2023-09-11.